IJMMM International Journal of Minerals, Metallurgy and Materials 矿物冶金与材料学报（英文版）

Effect of nonmetallic inclusions on localized corrosion of spring steel

Wei-ning Shi, Shu-feng Yang, and Jing-she Li

Cite this article as:
Wei-ning Shi, Shu-feng Yang, and Jing-she Li, Effect of nonmetallic inclusions on localized corrosion of spring steel, *Int. J. Miner. Metall. Mater.*, 28(2021), No. 3, pp. 390-397. https://doi.org/10.1007/s12613-020-2018-z

International Journal of Minerals, Metallurgy and Materials
Volume 28, Number 3, March 2021, Page 390
https://doi.org/10.1007/s12613-020-2018-z

Effect of nonmetallic inclusions on localized corrosion of spring steel

Wei-ning Shi, Shu-feng Yang, and Jing-she Li

School of Metallurgical and Ecological Engineering, University of Science and Technology Beijing, Beijing 100083, China
(Received: 3 December 2019; revised: 10 February 2020; accepted: 11 February 2020)

Abstract: Certain inclusions in high-strength 60Si2Mn–Cr spring steel result in poor resistance to localized corrosion. In this work, to study the effect of inclusions on the localized corrosion behavior of spring steel, accelerated corrosion tests were performed by immersing spring steel in 3wt% $FeCl_3$ solution for different times. The results show that severe corrosion occurred in areas of clustered CaS inclusions. Sulfide inclusions containing Ca and Mg induced the strongest localized corrosion susceptibility. For the case of (Ca,Mn,Mg)S inclusions, the ability to induce localized corrosion susceptibility is ranked as follows: MgS > CaS > MnS. Moreover, CaS, (Ca,Mn)S, and (Ca,Mn,Mg)S inclusions were mainly responsible for inducing environmental embrittlement.

Keywords: steel; localized corrosion; inclusions; accelerated corrosion tests

1. Introduction

Lightweight and high-strength spring steels are required to meet the needs of the modern automotive industry and high-speed railways [1–2]. However, these advantages, especially those induced by the presence of nonmetallic inclusions, decrease the corrosion resistance of the steels [3–4]. The presence of inclusions, such as Al_2O_3, MnS, and composites, introduced by adding a deoxidizing agent during the steelmaking or refining process, destroys the metallic material due to an increase in cracking sources [5–8]. Fish-eye fractures are typically induced by oxide or TiN inclusions due to their capacity for hydrogen absorption [9–10]. Furthermore, a tiny change of state resulting from the presence of inclusions yields enormous impacts on material failure; moreover, corrosion pits form around the inclusions [11–13]. Nam *et al*. [14] reported that corrosion fatigue cracking emerged at the pitting sites of MnS inclusions because of anodic dissolution and hydrogen embrittlement. The types and states of inclusions mutually reinforce hydrogen absorption, which leads to hydrogen embrittlement. Komazaki *et al*. [15] illustrated that absorbed hydrogen and corrosion pits had the same impacts on environmental embrittlement (EE) in spring steel. The formation of corrosion pits, mainly initiated by inclusions, is the key factor leading to fracture failure in spring steel.

Different types of inclusions yield different localized corrosion susceptibilities [16]. The pitting corrosion mechanisms induced by various inclusions in stainless and pipeline steels have been comprehensively analyzed [16–18]. The passive film at the boundary of the inclusion and the matrix is generally susceptible to dissolution; therefore, the emerging fresh boundary undergoes pitting corrosion due to chemical inhomogeneity. Corrosion pits develop at the inclusion sites after both metastable and stable pitting [19–21]. However, studying the inclusion-induced localized corrosion behavior of spring steel is difficult because the matrix is susceptible to corrosion. Understanding this process of localized corrosion would clarify which inclusions need to be controlled in steelmaking or other metallurgical processes [22–24], so that the resistance to localized corrosion and EE is fundamentally improved.

To address this issue, in situ immersion tests were employed in this study to investigate the localized corrosion behaviors of 60Si2Mn–Cr spring steel induced by various inclusions. The inclusions were statistically detected and analyzed by scanning electron microscopy (SEM) coupled with energy-dispersive X-ray spectroscopy (EDS). Immersion tests in 3wt% $FeCl_3$ solution (298 K) were then conducted.

2. Experimental

The experimental material was 60Si2Mn–Cr spring steel, the chemical composition of which has been previously reported [4]. The as-cast steel specimens were employed prior

Corresponding author: Shu-feng Yang E-mail: yangshufeng@ustb.edu.cn

to the experiments in order to exclude the influence of other factors (heat, deformation treatment) on the inclusion-induced localized corrosion behavior of spring steel [25]. The standard corrosion specimen size was 10 mm × 10 mm × 5 mm. Immersion tests were conducted in 3wt% $FeCl_3$ solution at 298 K. All specimens were ground with 2000-grit silicon carbide paper and polished with 0.5 μm-diameter-particle diamond paste to avoid the effects of surface roughness. The specimens were then rinsed using deionized water, degreased using alcohol, and dried immediately. The morphologies and compositions of the inclusions were analyzed by a Phenom ProX scanning electron microscope using backscatter electron imaging and EDS modes, respectively. The type, composition, size, number, and distribution of inclusions were analyzed by SEM. Ninety inclusions were randomly selected in each specimen to record their positions and statistically identify their properties. Image-Pro image-processing software (Media Cybernetics, USA) was employed to calculate the average size of the inclusions. Each test was repeated three times to ensure accuracy of the calculations.

Immersion tests were conducted in 3wt% $FeCl_3$ solution with immersion times of 0 s, 5 s, and 15 s to analyze the localized corrosion behaviors of 60Si2Mn–Cr spring steel induced by various inclusions. Other surfaces were sealed with epoxy resin to achieve a faultless test surface and suppress the impacts of specimen defects on the corrosion behavior. Pure hydrated $FeCl_3$ and deionized water were used to prepare the immersion solution.

3. Results

The distribution (Fig. 1(a)) and the number proportion and average size (Fig. 1(b)) of various inclusions (their compositions were determined by SEM-EDS) were studied. Fig. 1(a) shows that MnS inclusions were uniformly distributed (#13). The MnS inclusions readily induced pitting corrosion because preferential dissolution around the sulfide inclusion can produce sulfur, which facilitates pitting initiation and propagation [26]. Moreover, TiN inclusions were the second most prevalent type and were also uniformly distributed (#12). Ha *et al*. [27] showed that inclusions containing more Ti and less content of Ca were resistant to corrosion. The dispersed distribution of TiN inclusions resulted in a slight susceptibility of the matrix to localized corrosion. In addition, CaS inclusions were unequally distributed and clustered (#11). Numerous CaS inclusions were present in the matrix and their corrosion resistance was much weaker than those of the other inclusions because of their sulfide nature and higher Ca content. The uneven distribution of CaS inclusions led to unequal corrosion because relatively dense areas of CaS inclusions yielded more severe localized corrosion. Composite (Ca,Mn)S inclusions displayed a non-clustered distribution (#10). Silicon carbide inclusions were uniformly distributed (#9), and their ability to improve corrosion resistance was much stronger than that of the sulfide inclusions due to the high Si content [28]. A relatively small proportion of (Ca,Mn,Mg)S inclusions was also present, and these presented a non-clustered distribution (#8); however, this type of inclusion enhanced the localized corrosion susceptibility of the steel matrix because of its high Ca and Mg contents. Few iron carbide inclusions (#7) exhibiting higher corrosion resistance were found in the matrix. Very few spinel and Al_2O_3 inclusions (#5, #6) existed in the matrix; thus, these had little effect on the localized corrosion of spring steel.

Fig. 1(b) shows that the proportion of single MnS inclusions (#13) reached almost one-half of all inclusions. Moreover, TiN (#12) and CaS inclusions (#11) were the second and third most common types, respectively. The res-

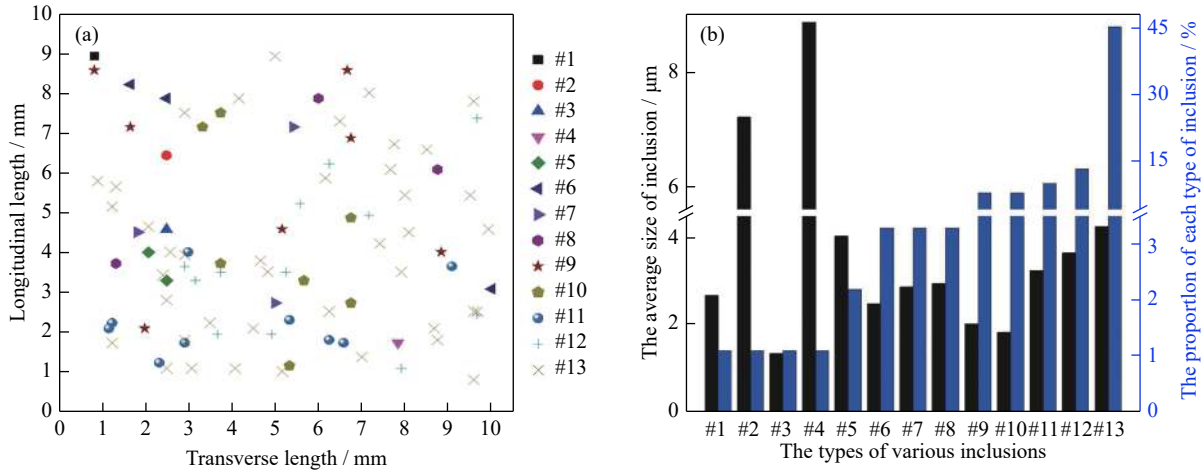

Fig. 1. Distribution (a) and proportion and average size (b) of inclusions in spring steel. #1—(Mg,Mn)S; #2—Al_2O_3+SiC; #3—Al_2O_3+MnS; #4—MgO+SiC; #5—Al_2O_3; #6—Al_2O_3+MgO; #7—iron carbide; #8—(Ca,Mn,Mg)S; #9—SiC; #10—(Ca,Mn)S; #11—CaS; #12—TiN; #13—MnS.

ults indicate that the sulfide inclusions and their composites were the dominant inclusions (#1, #3, #8, #10, #11, #13) present in the matrix, accounting for 68.13% of all inclusions. Because these inclusions can induce localized corrosion in spring steel, the corrosion resistance was significantly decreased. The average sizes of the sulfide, oxide, and other inclusions were 2.9, 4.98, and 4.9 μm, respectively. The average size of the composite-sulfide inclusions (#1, #3, #8, #10) was smaller than that of the single-sulfide inclusions (#11, #13); therefore, these small-sized composites improved the corrosion resistance. Studies have shown that the corrosion resistance around an inclusion is governed by the micro-crevice formed at the inclusion/matrix boundary and by the critical size of the inclusion: specifically, a smaller-sized inclusion improves localized corrosion resistance [29–32]. The small-sized SiC (#9) and TiN inclusions (#12) therefore provided better localized corrosion resistance than the composite oxide (#2, #4, #5) or sulfide inclusions (#13). Accelerated corrosion tests were performed in 3wt% $FeCl_3$ solution for immersion times of 0 s, 5 s, and 15 s to observe the localized corrosion behaviors of spring steel induced by various inclusions. The localized corrosion behavior around MnS inclusions was preferentially analyzed due to their greater number (as shown in Fig. 1). The results showed that the average size of MnS inclusions was 4.3 μm, and the majority of these exhibited polygonal morphology. The corrosion morphologies of MnS inclusions before and after corrosion tests, shown in Figs. 2(a)–2(c), indicate that these inclusions dissolved at the inclusion/matrix boundary after an immersion time of 5 s. A micro-crevice at the inclusion/matrix boundary was formed after 15 s, as indicated by the increase in the image contrast, and no dissolution was found on the surface of these inclusions. This shows that the pitting initiation process occurred along the depth direction at the inclusion/matrix boundary. The corrosion morphologies of TiN inclusions before and after the immersion tests are shown in Figs. 2(d)–2(f). The TiN inclusions were not dissolved after 15 s, but their average size (~3.6 μm) was small, which illustrates relatively higher localized corrosion resistance compared with that of other inclusions.

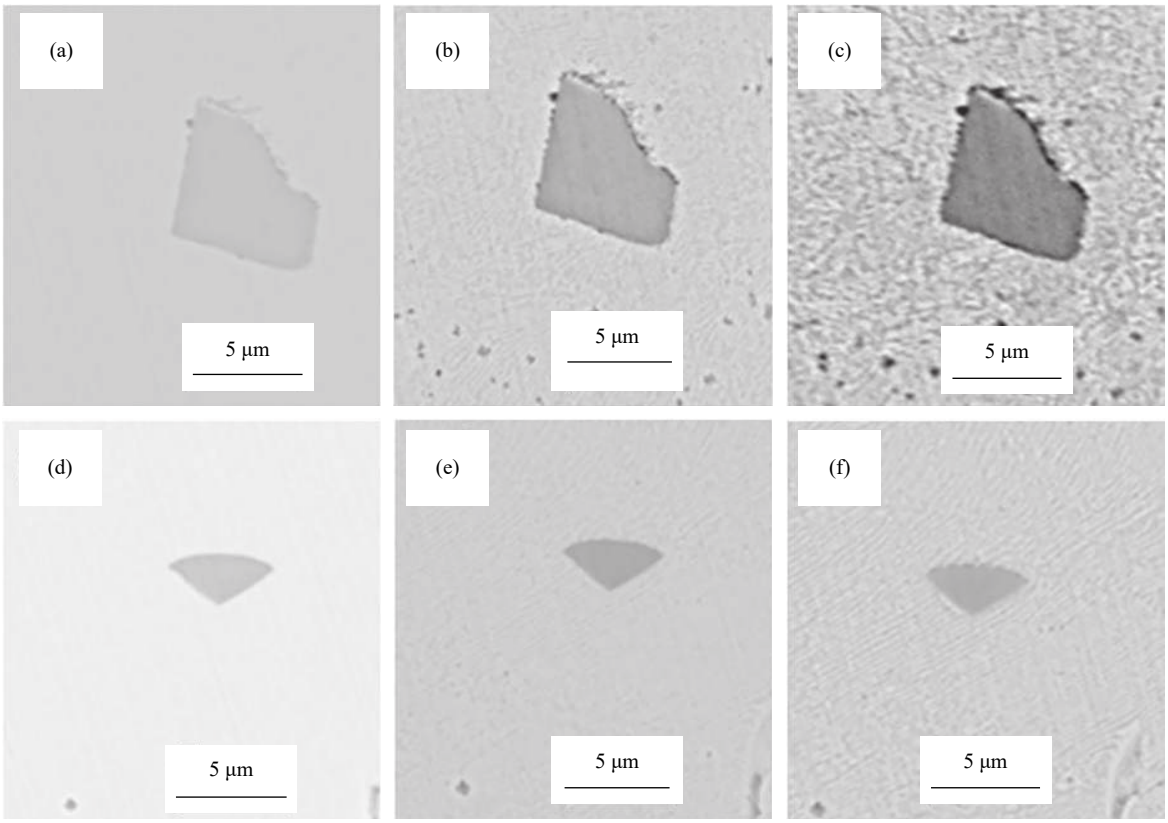

Fig. 2. Corrosion morphologies of MnS (a–c) and TiN inclusions (d–f) after immersion times in 3wt% $FeCl_3$ solution: (a) and (d) 0 s; (b) and (e) 5 s; (c) and (f) 15 s.

Corrosion morphologies of CaS inclusions after immersion times of 0, 5, and 15 s in 3wt% $FeCl_3$ solution are shown in Fig. 3. The chemical compositions detected by SEM-EDS of CaS inclusions after different immersion times are shown in the table of Fig. 3(d). By increasing the immersion time to 5 s, the contents of S and Ca in CaS inclusion were reduced (Fig. 3(b)). Moreover, CaS inclusion was completely dissolved after an immersion time of 15 s (Fig. 3(c)) since the S

and Ca contents in CaS inclusion monotonically decreased to 0, as shown in the table of Fig. 3(d). Compared with the results of Fig. 2, the corrosion resistance of the steel matrix around CaS inclusions was weaker than that of the steel matrix around MnS inclusions. The corrosion morphology of (Ca,Mn)S inclusions is shown in Fig. 4. The CaS inclusions in these composites dissolved entirely, leaving a residue of MnS after an immersion time of 5 s. This then completely dissolved at 15 s. Comparing the results of Figs. 2(a)–2(c) with those of Fig. 4, the presence of CaS inclusions in (Ca,Mn)S composite inclusions weakened the corrosion resistance of MnS inclusions.

The corrosion morphologies of (Ca,Mn,Mg)S inclusions (~3 μm) before and after immersion tests are shown in Fig. 5.

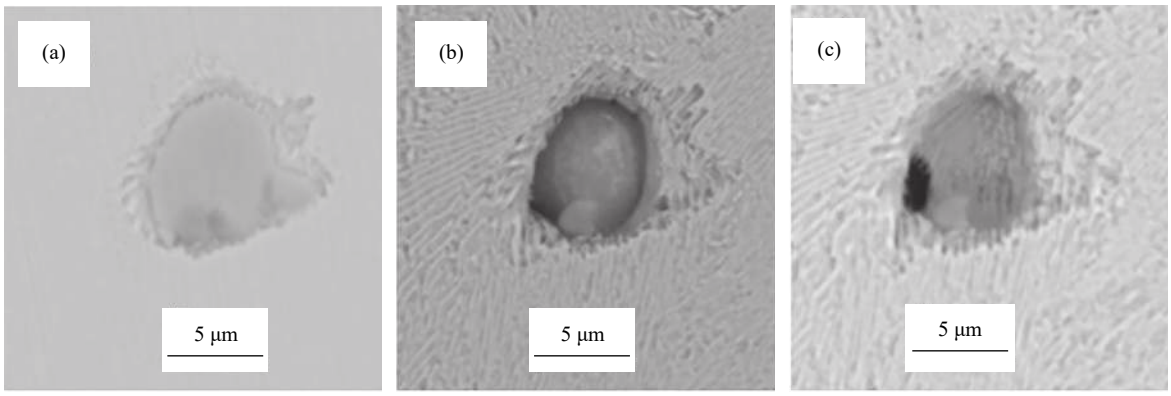

(d)

Immersion time / s	Chemical composition / wt%		
	S	Ca	Fe
0	28.3	30.2	41.5
5	13.5	27.0	59.5
15	0	0	100.0

Fig. 3. Corrosion morphologies after immersion times of 0 s (a), 5 s (b), and 15 s (c) in 3wt% $FeCl_3$ solution and corresponding compositions (d) of CaS inclusions.

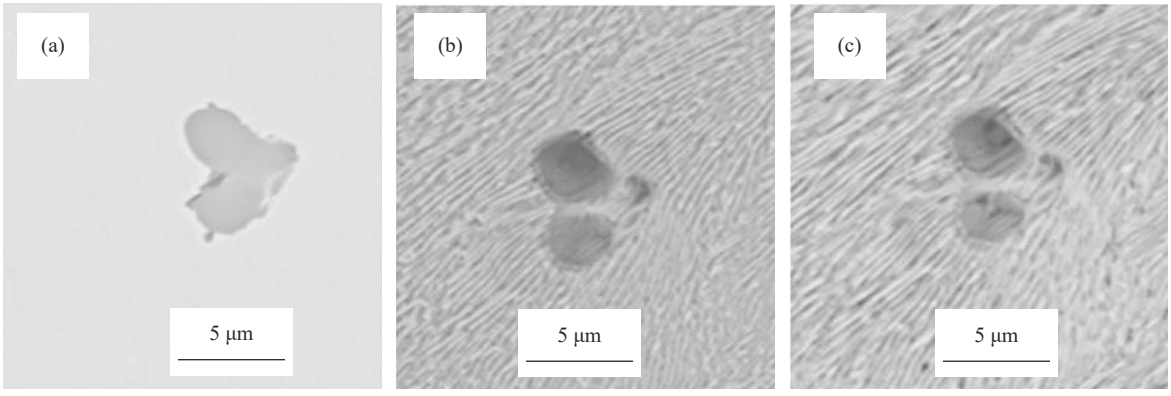

(d)

Immersion time / s	Chemical composition / wt%			
	S	Mn	Ca	Fe
0	25.9	16.6	21.3	36.2
5	8.1	13.9	0	78.0
15	0	0	0	100.0

Fig. 4. Corrosion morphologies after immersion times of 0 s (a), 5 s (b), and 15 s (c) in 3wt% $FeCl_3$ solution and corresponding compositions (d) of (Ca,Mn)S inclusions.

The MgS inclusions in this composite were preferentially and entirely dissolved at the immersion time of 5 s, leaving a remnant composition of (Ca,Mn)S. The CaS component then dissolved entirely at 15 s, leaving only MnS. Fig. 6 shows the elemental mapping result of (Ca,Mn,Mg)S inclusion after an immersion time of 15 s in 3wt% $FeCl_3$ solution, corresponding to Fig. 5(c). The MgS and CaS components dissolved in an orderly manner when compared with the case of Fig. 5, leaving only MnS inside the pits after an immersion time of 15 s. Figs. 2(a)–2(c) and Figs. 4–6 show that the presence of

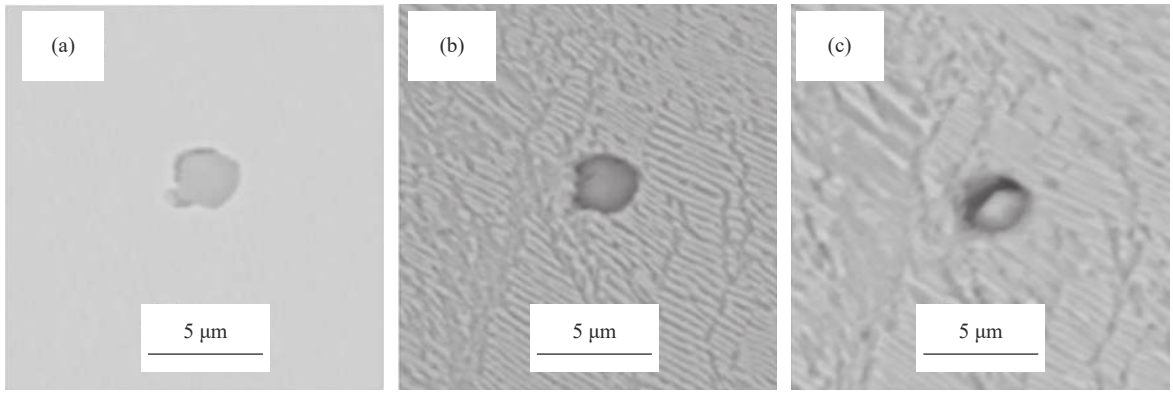

(d)

Immersion time / s	Chemical composition / wt%				
	S	Mn	Ca	Mg	Fe
0	23.6	29.4	4.9	3.7	38.4
5	15.5	34.5	4.6	0	45.4
15	18.3	31.7	0	0	50.0

Fig. 5. Corrosion morphologies after immersion times of 0 s (a), 5 s (b), and 15 s (c) in 3wt% $FeCl_3$ solution and corresponding compositions (d) of (Ca,Mn,Mg)S inclusions.

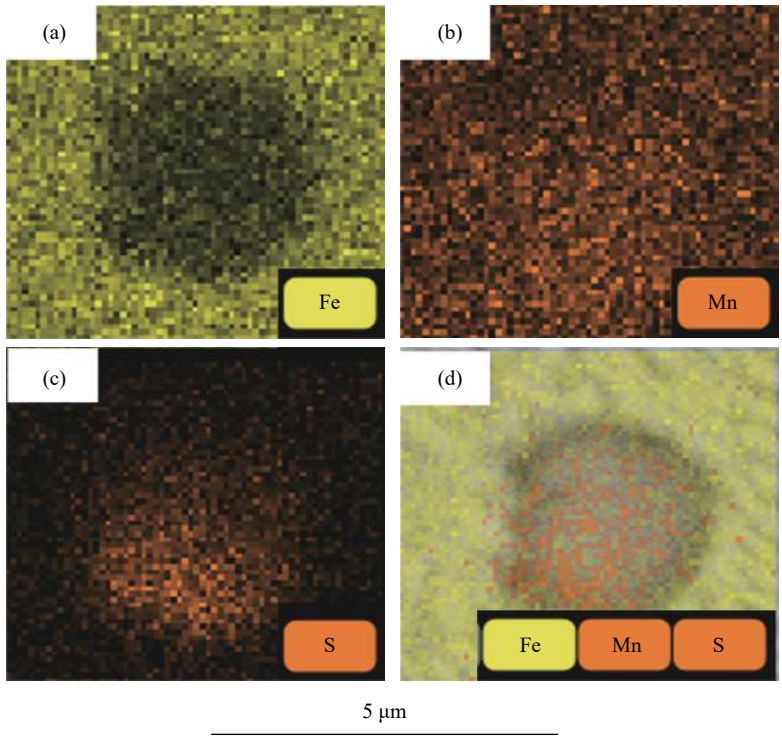

Fig. 6. Elemental mapping result of (Ca,Mn,Mg)S inclusion after an immersion time of 15 s in 3wt% $FeCl_3$ solution: (a) Fe; (b) Mn; (d) S; (d) combination of Fe, Mn, and S.

Mg in composite inclusions changed the localized corrosion resistance of the steel matrix around both MnS and CaS inclusions. A competitive corrosion relationship existed between the components of the MgS, CaS, and MnS inclusions in (Ca,Mn,Mg)S composites. The MgS inclusions in composites dissolved preferentially, and the corrosion process of other compositions was relatively delayed.

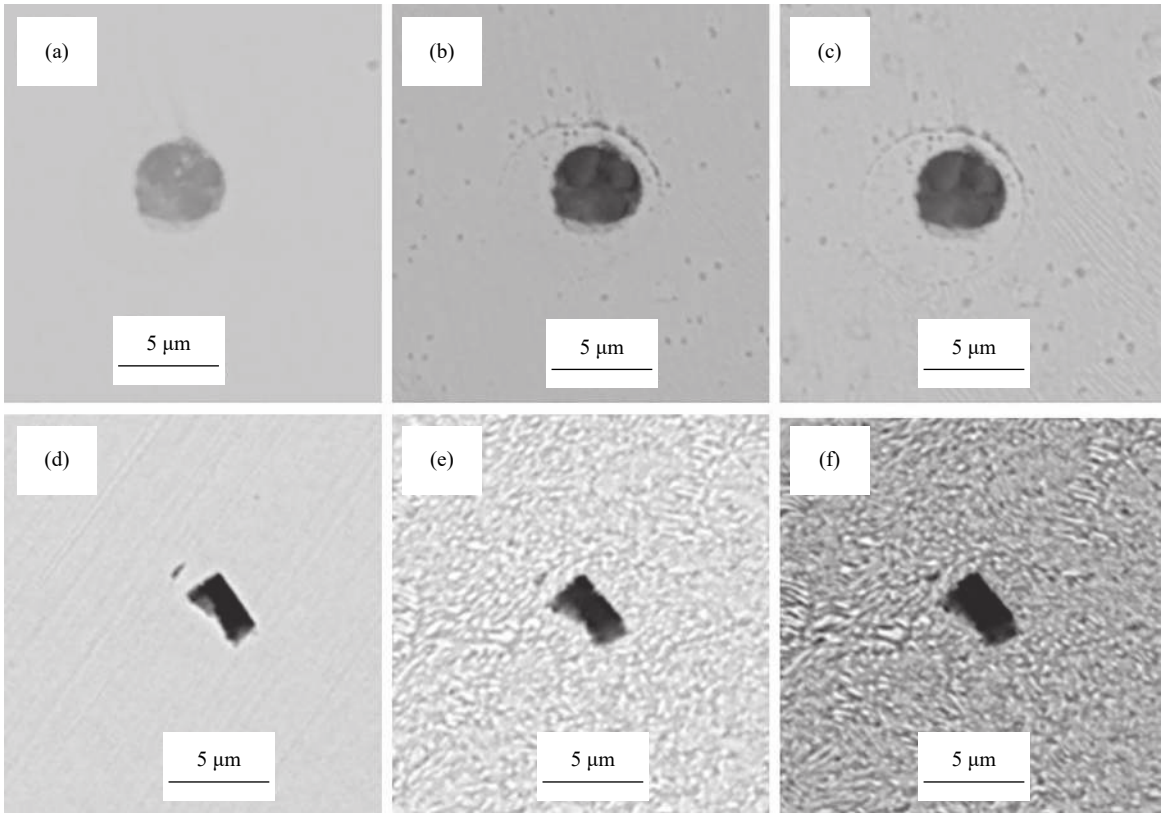

Fig. 7. Corrosion morphologies of iron carbide (a–c) and SiC inclusions (d–f) after immersions in 3wt% $FeCl_3$ solution: (a) and (d) 0 s; (b) and (e) 5 s; (c) and (f) 15 s .

The corrosion morphologies of iron carbide inclusions before and after immersion tests are shown in Figs. 7(a)–7(c). The local matrix around these inclusions possessed strong corrosion resistance because no dissolution occurred after an immersion time of 15 s. The corrosion morphologies of SiC inclusions before and after immersion tests are shown in Figs. 7(d)–7(f). The corrosion behavior of SiC inclusions was similar to that of iron carbide, and no dissolution occurred, regardless of whether the matrix underwent serious corrosion, even at an immersion time of 15 s. This suggested that the steel matrix acted as a soluble anode and the dissolution potential of SiC inclusions was relatively high. Other inclusions were not analyzed owing to their extremely low proportion in the specimen. They also had no significant effect on the localized corrosion behavior of 60Si2Mn–Cr spring steel.

Fig. 8 shows a typical macroscopic view of the corrosion morphology of spring steel after immersion in 3wt% $FeCl_3$ solution for 15 s. Fig. 8(a) shows that there were two separate areas in the matrix, labeled as the clustered and dispersed CaS inclusion areas. The clustered CaS inclusion area had a more severe corrosion than the dispersed area. Fig. 8(b) indicates that the clustered CaS inclusions induced a tunnel ef-

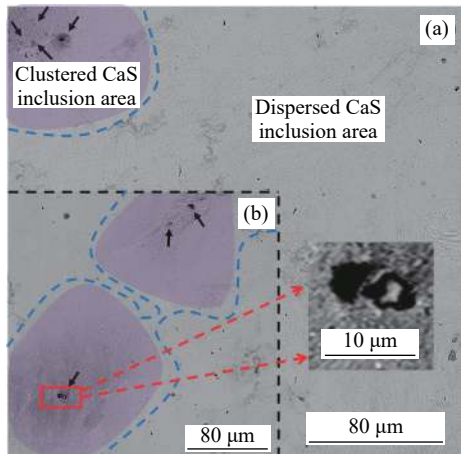

Fig. 8. Corrosion morphologies of clustered and dispersed CaS inclusion areas. The purple areas in (a) and (b) show the clustered CaS inclusion area. The red dashed arrows refer to the enlarged view in the red solid frame.

fect, which triggered severe corrosion below the matrix surface, irrespective of the surface state.

4. Discussion

The distribution, number, size, type, and composition of various inclusions in spring steel affected the formation of corrosion pits. Figs. 1 and 8 show that the clustered area of CaS inclusions induced many pits due to their tunnel effect. A large proportion of clustered CaS inclusion areas would trigger severe exfoliation behavior. In contrast, the areas of dispersed CaS inclusions had no serious corrosion because of the existence of a complete entity below the surface. Figs. 2–7 show that the local matrix around composites containing CaS, MnS, and MgS inclusions possessed a stronger localized corrosion susceptibility. The MgS inclusions preferentially dissolved, followed by CaS inclusions, while MnS inclusions were the last to dissolve. The localized corrosion susceptibility around these three sulfide inclusions is therefore ranked as MgS > CaS > MnS. The localized corrosion susceptibilities around TiN, SiC, and iron carbide inclusions were relatively low (Figs. 2(d)–2(f) and 7), despite their high proportion in the steel (Fig. 1). Corrosion pits were therefore likely to occur at sites of sulfide and composite inclusions. Moreover, CaS, (Ca,Mn)S, and (Ca,Mn,Mg)S inclusions accounted for a large proportion (Fig. 1(b)) of the total inclusions, and their abilities to induce localized corrosion was very strong (Figs. 3–6). This indicated that corrosion pits in this spring steel were mainly induced by these three types of inclusions, despite that the pits appeared shallow due to the very thin surface presented by the three-dimensional inclusions after the grinding and polishing of the specimens. Therefore, we conclude that CaS, (Ca,Mn)S, and (Ca,Mn,Mg)S inclusions in spring steel mainly induce EE. If these three types of inclusions can be well controlled to yield a dispersed distribution of CaS inclusions or even be removed during steelmaking or other metallurgical process [33], the corrosion pits would be significantly reduced and resistance to EE could be fundamentally improved.

5. Conclusions

(1) The proportions of various inclusions in the matrix of spring steel are ordered as follows: MnS > TiN, SiC, iron carbide > sulfides containing Ca or Mg > composite oxide. The localized corrosion resistances of the local steel matrices around TiN, SiC, and iron carbide inclusions were greater than those of the other main inclusions. Sulfide inclusions containing Ca and Mg caused the worst localized corrosion resistance of spring steel.

(2) Clustered CaS inclusion areas triggered a corrosion tunnel effect, causing corrosion pits to form, even below the surface. In contrast, dispersed CaS inclusion areas showed slight corrosion due to the existence of the complete entity below the surface. For the case of (Ca,Mn,Mg)S inclusions, the ability to induce localized corrosion susceptibility is ranked as follows: MgS > CaS > MnS.

(3) Lastly, CaS, (Ca,Mn)S, and (Ca,Mn,Mg)S are the main inclusion types in spring steel that induce EE. Removing these three inclusion types and dispersing the clustered areas of CaS inclusions in the steelmaking or refining process would improve resistance to EE.

Acknowledgements

The authors are grateful for support from the National Natural Science Foundation of China (Nos. 51574190, 51734003 and 51874116) and Fundamental Research Funds for the Central Universities (No. FRF-TP-18-009C1).

References

[1] G. Niu, Y.L. Chen, H.B. Wu, X. Wang, and D. Tang, Corrosion behavior of high-strength spring steel for high-speed railway, *Int. J. Miner. Metall. Mater.*, 25(2018), No. 5, p. 527.

[2] V.I. Zurnadzhy, V.G. Efremenko, K.M. Wu, A.Y. Azarkhov, Y.G. Chabak, V.L. Greshta, O.B. Isayev, and M.V. Pomazkov, Effects of stress relief tempering on microstructure and tensile/impact behavior of quenched and partitioned commercial spring steel, *Mater. Sci. Eng. A*, 745(2019), p. 307.

[3] R. Wang, Y.P. Bao, Y.H. Li, Z.J. Yan, D.Z. Li, and Y. Kang, Influence of metallurgical processing parameters on defects in cold-rolled steel sheet caused by inclusions, *Int. J. Miner. Metall. Mater.*, 26(2019), No. 4, p. 440.

[4] W.N. Shi, S.F. Yang, A.P. Dong, and J.S. Li, Understanding the corrosion mechanism of spring steel induced by MnS inclusions with different sizes, *JOM*, 70(2018), No. 11, p. 2513.

[5] Y. Hu, W.Q. Chen, C.J. Wan, F.J. Wang, and H.B. Han, Effect of deoxidation process on inclusion and fatigue performance of spring steel for automobile suspension, *Metall. Mater. Trans. B*, 49(2018), No. 2, p. 569.

[6] R. Wang, Y.P. Bao, Z.J. Yan, D.Z. Li, and Y. Kang, Comparison between the surface defects caused by Al_2O_3 and TiN inclusions in interstitial-free steel auto sheets, *Int. J. Miner. Metall. Mater.*, 26(2019), No. 2, p. 178.

[7] C. Gu, Y.P. Bao, P. Gan, M. Wang, and J.S. He, Effect of main inclusions on crack initiation in bearing steel in the very high cycle fatigue regime, *Int. J. Miner. Metall. Mater.*, 25(2018), No. 6, p. 623.

[8] S. Lyu, X.D. Ma, Z.Z. Huang, Z. Yao, H.G. Lee, Z.H. Jiang, G. Wang, J. Zou, and B.J. Zhao, Understanding the formation and evolution of oxide inclusions in Si-deoxidized spring steel, *Metall. Mater. Trans. B*, 50(2019), No. 4, p. 1862.

[9] S.K. Dwivedi and M. Vishwakarma, Hydrogen embrittlement in different materials: a review, *Int. J. Hydrogen Energy*, 43(2018), No. 46, p. 21603.

[10] M. Kubota, T. Suzuki, D. Hirakami, and K. Ushioda, Influence of hydrogen on fatigue property of suspension spring steel with artificial corrosion pit after multi-step shot peening, *ISIJ Int.*, 55(2015), No. 12, p. 2667.

[11] U. Zerbst, M. Madia, C. Klinger, D. Bettge, and Y. Murakami, Defects as a root cause of fatigue failure of metallic compon-

ents. III: Cavities, dents, corrosion pits, scratches, *Eng. Fail. Anal.*, 97(2019), p. 759.
[12] J.J. Shi, J. Ming, and Xin Liu, Pitting corrosion resistance of a novel duplex alloy steel in alkali-activated slag extract in the presence of chloride ions, *Int. J. Miner. Metall. Mater.*, 24(2017), No. 10, p. 1134.
[13] Y.Z. Ma, C.L. Yang, Y.J. Liu, F.S. Yuan, S.S. Liang, H.X. Li, and J.S. Zhang, Microstructure, mechanical, and corrosion properties of extruded low-alloyed Mg–*x*Zn–0.2Ca alloys, *Int. J. Miner. Metall. Mater.*, 26(2019), No. 10, p. 1274.
[14] T.H. Nam, M.S. Kwon, and J.G. Kim, Mechanism of corrosion fatigue cracking of automotive coil spring steel, *Met. Mater. Int.*, 21(2015), No. 6, p. 1023.
[15] S. Komazaki, K. Kobayashi, T. Misawa, and T. Fukuzumi, Environmental embrittlement of automobile spring steels caused by wet–dry cyclic corrosion in sodium chloride solution, *Corros. Sci.*, 47(2005), No. 10, p. 2450.
[16] L.W. Wang, J.C. Xin, L.J. Cheng, K. Zhao, B.Z. Sun, J.R. Li, X. Wang, and Z.Y. Cui, Influence of inclusions on initiation of pitting corrosion and stress corrosion cracking of X70 steel in near-neutral pH environment, *Corros. Sci.*, 147(2019), p. 108.
[17] B.W. Luo, J. Zhou, P.P. Bai, S.Q. Zheng, T. An, and X.L. Wen, Comparative study on the corrosion behavior of X52. 3Cr.and 13Cr steel in an O_2–H_2O–CO_2 system: products. reaction kinetics.and pitting sensitivity, *Int. J. Miner. Metall. Mater.*, 24(2017), No. 6, p. 646.
[18] W.N. Shi, S.F. Yang, and J.S. Li, Correlation between Cr-depleted zone and local corrosion in stainless steels: a review, *J. Chin. Soc. Corros. Prot.*, 39(2019), No. 4, p. 281.
[19] Y.T. Zhou, S.J. Zheng, B. Zhang, and X.L. Ma, Atomic scale understanding of the interaction between alloying copper and MnS inclusions in stainless steels in NaCl electrolyte, *Corros. Sci.*, 111(2016), p. 414.
[20] R.L. Liu, T.S. Li, L. Liu, Y. Cui, E.E. Oguzie, Y. Li, and F.H. Wang, Cellular automata study of the combined effects of passive film breakdown and repassivation on metastable pits on sputtered nanocrystalline stainless steel, *J. Electrochem. Soc.*, 166(2019), p. 4.
[21] L. Sun, Y.T. Sun, Y.Y. Liu, N.W. Dai, J. Li, and Y.M. Jiang, Effect of annealing temperature on pitting behavior and microstructure evolution of hyper‐duplex stainless steel 2707, *Mater. Corros.*, 70(2019), No. 9, p. 1682.
[22] Y.F. Wang, G.X. Cheng, W. Wu, and Y. Li, Role of inclusions in the pitting initiation of pipeline steel and the effect of electron irradiation in SEM, *Corros. Sci.*, 130(2018), p. 252.
[23] H. Feng, Z.H. Jiang, H.B. Li, P.C. Lu, S.C. Zhang, H.C. Zhu, B.B. Zhang, T. Zhang, D. Xu, and Z.G. Chen, Influence of nitrogen on corrosion behaviour of high nitrogen martensitic stainless steels manufactured by pressurized metallurgy, *Corros. Sci.*, 144(2018), p. 288.
[24] H. Feng, H.B. Li, X.L. Wu, Z.H. Jiang, S. Zhao, T. Zhang, D.K. Xu, S.C. Zhang, H.C. Zhu, B.B. Zhang, and M.X. Yang, Effect of nitrogen on corrosion behaviour of a novel high nitrogen medium-entropy alloy CrCoNiN manufactured by pressurized metallurgy, *J. Mater. Sci. Technol.*, 34(2018), No. 10, p. 1781.
[25] L. Peguet, B. Malki, and B. Baroux, Influence of cold working on the pitting corrosion resistance of stainless steels, *Corros. Sci.*, 49(2007), No. 4, p. 1933.
[26] M.M. Nishimoto, I.S. Muto, Y. Sugawara, and N. Hara, Morphological characteristics of trenching around MnS inclusions in type 316 stainless steel: the role of molybdenum in pitting corrosion resistance, *J. Electrochem. Soc.*, 166(2019), No. 11, p. C3801.
[27] H.Y. Ha, C.J. Park, and H.S. Kwon, Effects of non-metallic inclusions on the initiation of pitting corrosion in 11% Cr ferritic stainless steel examined by micro-droplet cell, *Corros. Sci.*, 49(2007), No. 3, p. 1266.
[28] Y.B. Li, J. Liu, Y.D. Deng, X.P. Han, W.B. Hu, and C. Zhong, Ex situ characterization of metallurgical inclusions in X100 pipeline steel before and after immersion in a neutral pH bicarbonate solution, *J. Alloys Compd.*, 673(2016), p. 28.
[29] D. Guo, C.T. Kwok, and S.L.I. Chan, Spindle speed in friction surfacing of 316L stainless steel–How it affects the microstructure hardness and pitting corrosion resistance, *Surf. Coat. Technol.*, 361(2019), p. 324.
[30] G.J. Cai and Y.R. Huang, Effects of Ce addition on grain boundary character distribution corrosion behavior and impact toughness of AISI 204Cu stainless steel, *J. Mater. Eng. Perform.*, 28(2019), No. 6, p. 3683.
[31] H.X. Jia, X.W. Zhang, J.P. Xu, Y.P. Sun, and J.X. Li, Effect of hydrogen content and strain rate on hydrogen-induced delay cracking for hot-stamped steel, *Metals*, 9(2019), No. 7, p. 798.
[32] M. Wohlschlögel, R. Steegmüller, and A. Schüßler, Effect of inclusion size and distribution on the corrosion behavior of medical-device grade nitinol tubing, *J. Mater. Eng. Perform.*, 23(2014), No. 7, p. 2635.
[33] X.F. Bai, Y.H. Sun, R.M. Chen, Y.M. Zhang, and Y.F. Cai, Formation and thermodynamics of CaS-bearing inclusions during Ca treatment in oil casting steels, *Int. J. Miner. Metall. Mater.*, 26(2019), No. 5, p. 573.